Change in Surface Topography of Structural Steel Under Cyclic Plastic Deformation

Aleena Saleem, Hiroshi Tamura, and Hiroshi Katsuchi

Abstract This paper concerns the change in surface topography of structural steel subjected to cyclic plastic deformation considering variable surface conditions and steel types. Notched steel specimens are configured for conducting the experiment under large amplitude cyclic strain. Furthermore, a surface curvature method is proposed for the evaluation of plastic strain from the surface height data obtained by a laser scanner. To this aim, displacement-controlled low cycle fatigue (LCF) tests are performed on mechanically polished and blasted steel specimens. Surface textures are measured at the start and end of fatigue loading cycles and relevant roughness parameters are calculated. Additionally, numerical simulation is conducted for the validation of the strain evaluation method. Regarding the effect of surface finish, blasted specimen showed the lowest fatigue strength with the highest values of surface roughness and plastic strain than the mechanically polished specimens. Analysis results suggest that the roughness parameters can be used for the comprehensive steel surface characterization. Moreover, surface treatment significantly affects the phenomenon of fatigue crack initiation than the types of steel.

Keywords Low cycle fatigue · Cyclic plastic deformation · Plastic strain · Surface roughness

A. Saleem (✉) · H. Tamura · H. Katsuchi
Department of Civil Engineering, Yokohama National University, Yokohama 240-8501, Japan
e-mail: aleena-saleem-ym@ynu.jp

H. Tamura
e-mail: tamura-hiroshi-jg@ynu.ac.jp

H. Katsuchi
e-mail: katsuchi@ynu.ac.jp

M. Abdel Wahab (ed.), *Proceedings of the 9th International Conference on Fracture, Fatigue and Wear*, Lecture Notes in Mechanical Engineering,
https://doi.org/10.1007/978-981-16-8810-2_14

1 Introduction

These days, surroundings are full of steel structures consisting of buildings and bridges playing an important role in our lives. Nevertheless, earthquakes can cause significant damages to the structural steel members resulting in loss of lives and properties. Although it is not possible to prevent the occurrence of earthquakes, the collapse of structures can be prevented. This can be achieved by understanding the behavior of steel undergoing earthquakes. In the fatigue process, continuous and repeated damage is confined to a specific area of the member undergoing stress and strain reversals. This phenomenon causes the accumulation of damage inside the material and finally, failure happens when a critical value of the damage is reached [1].

For metals undergoing cyclic plastic deformation, failure often occurs at less than 10^4 cycles and this phenomenon is considered as LCF [2]. This process results in repeated permanent material deformation under fatigue loading involving larger plastic strains and fewer cycles [3, 4]. Due to the recurrent yielding near the areas of higher stress concentrations such as holes, notches, weld toes, end of bridge piers, and beam-column connections, LCF arises. Alternating processes of tension and compression could result in the movement of dislocations. With time, these dislocations get accumulated and the cyclic hardening and softening phenomena occur [5]. In case of LCF, the failure process is governed by the plastic damage, and it can be illustrated by the deterioration of microstructure including void formation, growth, initiation, and propagation of microcracks. Structures experience higher strain rates and larger plastic strain at the local areas of steel members [6]. In the past, brittle fractures originating from ductile crack initiation were observed in beam-column connections and bridge piers during the Kobe earthquake of 1995 in Japan [7, 8]. Also, similar damages were visualized during the Northridge earthquake of 1994 in the United States [9].

Regarding the LCF life prediction, Miner's rule [10] is widely used for the prediction of crack initiation on the steel surface. Additionally, some other studies were conducted on LCF incorporating the variable parameters of strain rates and strain amplitudes by the modification of Miner's rule [11, 12]. However, these formulas were obtained from the experimentation incorporating some of the material constants, and further experimental work is required to cover various conditions of actual steel structures by considering the combined effects of variable surface finishes, steel properties, strain amplitudes, and strain rates. Nevertheless, considering the past literature, limited research is available on conducting LCF testing under large amplitude cyclic plastic strain. Also, it is important to investigate the effect of all the above-mentioned parameters on fatigue life for limiting the brittle fractures of steel structures.

Surface finish is an important parameter influencing the fatigue strength of steel. A component from a structure or machine will have variable surface finishes and various fatigue strengths [13]. Al-Shahrani and Marrow [14] checked the effect of surface modification on the fatigue limit of austenitic stainless steel and it was found that the residual stress on the specimen's surface is a dominant parameter affecting the

fatigue strength. In the LCF regime, cracks often start to initiate from the surface of metals. Therefore, the parameter of surface roughness is important in characterizing the surface geometry and the process of crack initiation [15]. Xiao et al. [16] approximated the power function relationship between fatigue strength and roughness by fitting the experimental data. A quantitative relationship was observed between both the parameters. Additionally, Gao et al. [17] studied the influence of microhardness, surface roughness, and residual stress of nickel aluminum bronze alloy on the fatigue life. The results highlighted that not only the compressive residual stress but also the factor of surface roughness induced by laser shock peening were the major parameters that affected the strength of the bronze alloy.

Furthermore, other investigations and analyses were done on the process of crack initiation in notched specimens. In the study of Leidermark et al. [18], fatigue life function was determined by conducting experiments on smooth and notched specimens. It was concluded that the fatigue notch factor should be well addressed to get a better comparison of numerical and experimental results. Hsu and Wang [19] examined the effects of crack initiation on specimens with variable heat treatments by employing finite element modeling. Experimental results demonstrated that the process of crack initiation was associated with the localization of plastic deformation. The above review signifies that the phenomenon of change in steel surface geometry leading to the initiation of cracks under LCF is needed to be further explored.

This paper focuses on topographic changes occurring on steel surfaces under repeated cyclic plastic deformation. Notched steel specimens with different loading conditions are designed for the application of large amplitude cyclic strain. Also, a surface curvature method is proposed for the evaluation of plastic strain from the surface height data. Specimens consisting of two types of test steels, S400 and S490 with mechanically polished and blasted finishes are used to study the variations in surface geometries under cyclic loading. To reveal the significant change in fatigue life, roughness parameters are evaluated at the start and end of loading cycles. Subsequently, the numerical simulation is done for the validation of experimental results.

2 Experiment Generating Large Cyclic Deformation

2.1 Material and Surface Finish

The materials used for the development of specimens are S400 and S490 test steels taken from Japanese Industrial Standards (JIS) [20]. For the test steels S400 and S490, the steel grades of SM400A and SM490A are used, respectively. Tensile tests are conducted on coupons for determining the mechanical properties. Table 1 enlists the mechanical and chemical properties of steels to be examined in the experimentation.

Table 1 Material properties of SM400A and SM490A steels

Steel grade	Yield stress (MPa)	Tensile stress (MPa)	Chemical Composition (%)				
			C	Mn	S	Si	P
SM400A	321	449	0.16	0.51	0.05	0.19	0.23
SM490A	367	539	0.16	1.49	0.002	0.35	0.016

Regarding the surface finish, specimens with mechanically polished and blasted surfaces are examined in this research study. In the first case, surfaces are mechanically polished by using White Alundum with abrasive count #46 in order to get a smooth surface. In the second case, blasting is done to remove corrosion from the metal's surface. Steel grit with abrasive count #100 is used for blasting treatment. Both the surface finishes are applied in the high strain region (at the center) of the specimen and the impact of initial residual stress is considered to be negligible.

2.2 Design Concept and Configuration of Testing Specimens

To produce the buckling phenomenon, notched steel specimens are developed for the current study. Figure 1 shows the top and side views of the designed specimen comprising of arc-shaped notches with a length of 280 mm and a width of 44 mm. Surface height measurements are done at the middle notch because of having no contact with side notches. In this study, cyclic compressive strain with a large amplitude is locally applied by using the buckling deformation of the steel specimens. This is done by grasping both ends of the flat plate specimens and then applying the repeated forced displacement. In this way, the large plastic strain will cause the formation of LCF cracks only at the center of steel specimens.

By the fatigue loading of the specimen, the phenomenon of surface geometry change leading to crack formation can be observed in detail since the largest strain will occur in the region (B) in each loading cycle. The following factors are considered for deciding the shape of the test specimen:

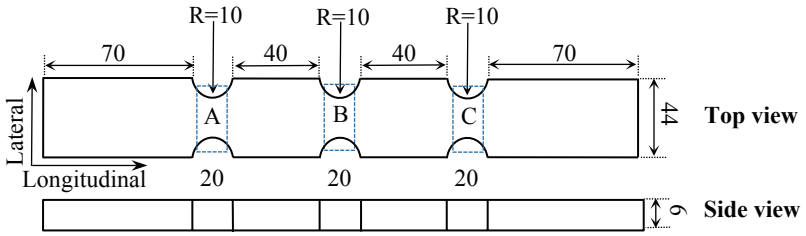

Fig. 1 Geometry of notched steel specimen (all dimensions are in mm)

1. To ensure the width of the specimen in the target area

   The width of the specimen in the notched part is chosen to be 20 mm so that the specimen remains in a uniaxial state of stress and the strain distribution is uniform in the width direction. Otherwise, the lesser width of the plate may cause the unequal distribution of strain and the specimen will be in a biaxial state of stress.
2. To fix the maximum strain amplitude generation region

   The surface finish is done at the center of the specimen on an area of 20×44 mm^2, so it is necessary to generate large amplitude plastic strain in the region (B) for the initiation of cracks at the same location. For this purpose, semicircular notches of similar dimensions are made in regions (A, B, and C) as marked in Fig. 1. After buckling, plastic hinges are formed in regions (A and C), and a significantly larger plastic strain occurs at the central notch in region (B). Since the maximum plastic strain due to bending is generated at the compression side of the central notch, surface geometry change can be easily observed in the area of interest.
3. To prevent the occurrence of fatigue cracks outside the focused region

   Since the large plastic strain is repetitively generated at the notches under fatigue loading, the radius of the notch is chosen not to be so small. If a fatigue crack initiates firstly in areas other than the focused region of interest, the behavior of the targeted area can be affected, or loading may be disturbed.
4. To reproduce the buckling deformation

   During the installation of the specimen in the testing machine, the buckling length of the specimen is kept constant irrespective of the depth of gripping the specimen's edge, so that the reproducibility of buckling deformation can be protected. This is achieved by developing arc-shaped notches with a radius of 10 mm.

2.3 Experimental Testing Procedure

Uniaxial and displacement-controlled fatigue loading having a triangular waveform with a constant amplitude of 5 mm is applied to the specimens. The history of input displacement with a triangular pattern is demonstrated in Fig. 2. The displacement rate is taken as 0.012 mm s^{-1}, so that the average strain rate is about 9.97×10^{-5} s^{-1} for the whole specimen. The lower end of the specimen is fixed, and the top end is movable in the longitudinal direction. The rotational freedom along the longitudinal direction at the top is relaxed, while the other two rotational degrees of freedom are fixed. Specimens are loaded using an MTS universal testing machine (810 Material Test System) having a loading capacity of 50 kN. Specimens are continued to be loaded until the appearance of visible cracks on the steel surface. A laser scanning

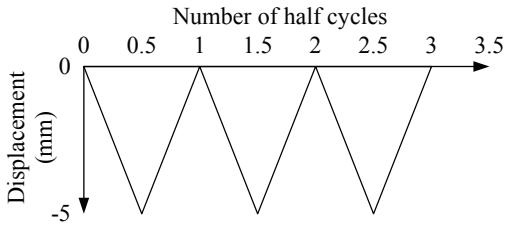

Fig. 2 History of input displacement for notched specimens

device (KEYENCE, LJ-V7080) is used to record the surface height data at the center of the specimen. The experimental testing setup is shown in Fig. 3.

For evaluating the combined effects of surface finish and steel type on LCF life and the process of crack initiation, different combinations of specimens are prepared as listed in Table 2. Specimens are named as FM-40-5 T, FM-49-5 T, and FB-49-5 T, where "FM" and "FB" represent the flat mirrored and flat blasted specimens respectively, "40" and "49" denote the SM400A and SM490A steels respectively, "5" is the displacement amplitude, and "T" represents the triangular loading waveform.

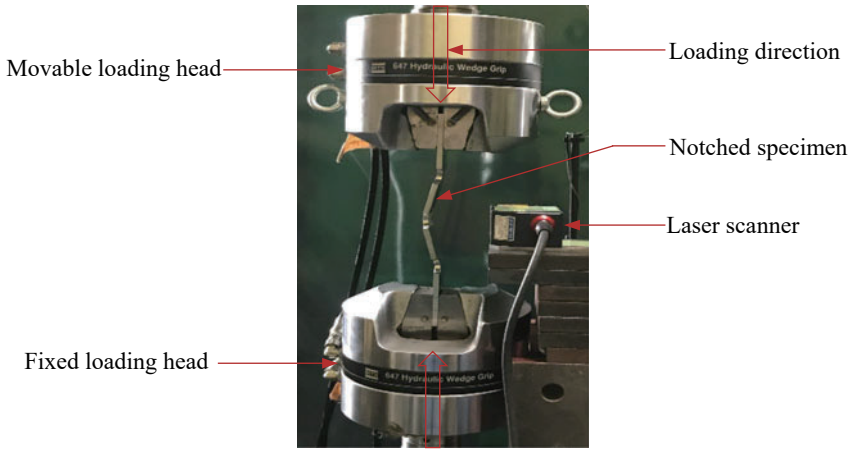

Fig. 3 Testing setup of the notched steel specimen

Table 2 Conditions of the test specimens

Specimen name	Steel type	Surface finish	Disp. amplitude (mm)
FM-40-5 T	SM400A	Mechanical polishing	5
FM-49-5 T	SM490A	Mechanical polishing	5
FB-49-5 T	SM490A	Blasting	5

3 Results and Discussions

As already described, all three specimens were loaded until the appearance of visible cracks at the middle notch. Table 3 enlists the number of cycles required for the initiation of cracks on all the test specimens. In the case of FB-49-5 T, cracks started to appear very earlier at 12.5 cycles than the mechanically polished specimens on which the cracks nucleated at 30.5 cycles.

3.1 Surface Curvature Method for Plastic Strain Evaluation

In the current experimentation, it was difficult to measure the plastic strain at the focused region (B) of the specimen because the strain gauge cannot be attached to the observation surface and the treated surfaces may also get damaged. Therefore, a surface curvature method is proposed for the evaluation of longitudinal strain from the surface height data obtained by the laser scanner. Data measurements are done on the compression side of the middle notch after each half cycle and then plastic strains are calculated. The point of strain evaluation is highlighted in Fig. 4.

The strain evaluation method is based on Euler–Bernoulli beam theory [21] and it can be given by following expressions:

$$\text{Radius of curvature} = \text{R} = \frac{(1 + (\text{z}')^2)^{3/2}}{|\text{z}''|} \tag{1}$$

$$\text{Bending strain} = \frac{\text{b}}{\text{R}} \tag{2}$$

where "z" is the surface height and "b" is the distance between the surface of steel from the neutral axis. In this method, firstly the surface height data at the compression side of the central notch is captured and then a polynomial fit is applied to the curve (in this research, an 8th-degree polynomial is used). After that the radius of curvature at the bottom of the curve is calculated and, ultimately the plastic strain is obtained

Table 3 Number of cycles required for the initiation of cracks

Specimen name	FM-40-5 T	FM-49-5 T	FB-49-5 T
Number of cycles	30.5	30.5	12.5

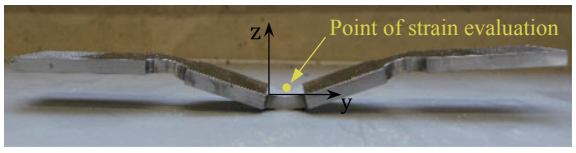

Fig. 4 Location of strain measurement at the compressive side of the middle notch

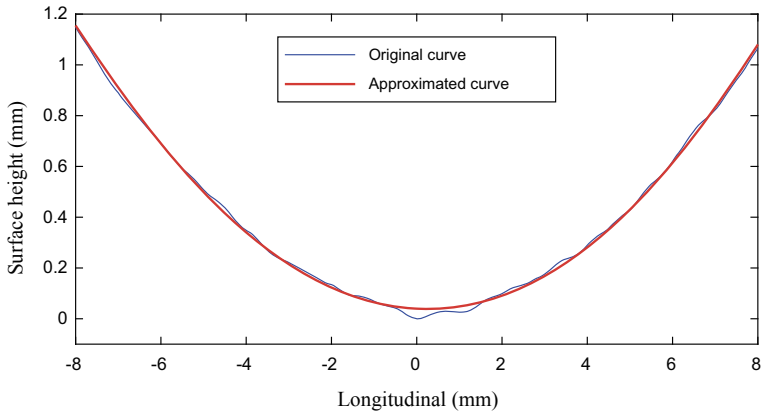

Fig. 5 An 8th order approximation of experimental surface height data ("Original curve" shows the original data and "Approximated curve" is used data for the evaluation of strain)

at the radius of curvature. However, the effects of axial strain and Poisson's ratio are ignored. By taking FM-40-5 ^{T} as an example, the original and 8th order approximated curves after 1.5 fatigue loading cycles are shown in Fig. 5. Here the horizontal axis with a longitudinal value of zero represents the center of the specimen.

Figure 6 explicates the histories of evaluated plastic strains for all the test specimens after each half cycle until the initiation of cracks. Black circles highlight the instant of crack identification on steel surfaces. In these figures, the "0.5" cycle is referred to as "compressive loading" and the "0.0" cycle is considered as "tensile loading". It is obvious from these results that the value of the plastic strain keeps on increasing with the progression in the number of loading cycles until the cracks appeared on the steel surface. This may be due to the residual plastic deformation accumulated after each fatigue loading cycle. Also, this increase can be attributed to the growing number of microcracks or the formation of cracks. After comparing the strain histories of FM-40-5 T and FM-49-5 T having the same surface finishes but different steel grades, it is observed that cracks appeared at 30.5 loading cycles for both the specimens. Also, the difference in strain values for both the specimens at the end of fatigue loading is very small showing that steel grade has less influence on fatigue life than that of surface finish. In the case of FB-49-5 T, cracks appeared earlier at 12.5 loading cycles with a plastic strain value of 17.97%. Surface blasting reduced the fatigue life by around 2.4 times that of mechanically polishing highlighting that surface treatment is an important parameter affecting the fatigue strength of steel structures. So much attention should be paid to the effect of surface finish for avoiding brittle failures.

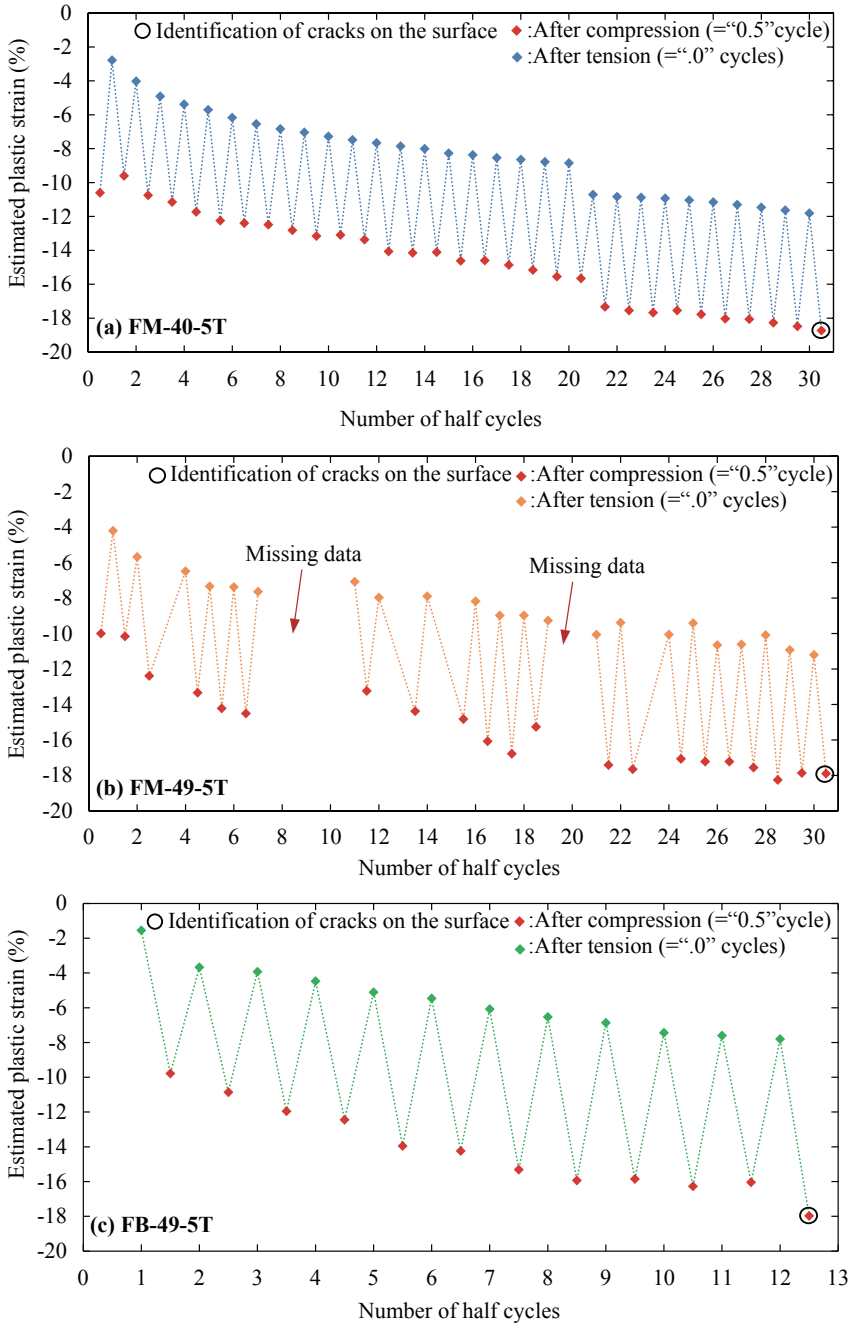

Fig. 6 Evaluated plastic strain histories for **a** FM-40-5 T, **b** FM-49-5 T and **c** FB-49-5 T

3.2 Surface Roughness Characterization

Fatigue cracks usually start to appear on the surface of the metals: thus, the surface treatment can greatly affect the fatigue life. Surface roughness parameters are commonly used for characterizing the topography of processed surfaces and their functionality-related properties can also be evaluated [22]. For the current experiment, surface textures are measured at the start and end of fatigue loading cycles by using a laser displacement meter from KEYENCE, Corporation, Japan. "Vision 64 Map" software by Bruker is used to conduct the surface topographic analyses over an area of 2×2 mm^2 at the center of the specimens. In the analysis process, after obtaining the raw surface height data, it is processed to remove outlier and waviness components in order to obtain a rough surface [23]. A Gaussian filter with a cutoff wavelength of 0.8 mm is applied both in longitudinal and lateral directions for eliminating the outlier, where the slope between the measured data points is 72.5° or more by using a Gaussian function. After that 4th-degree polynomial is applied for removing the curvature and finally the rough surface is attained.

Figure 7 demonstrates the three-dimensional (3D) steel surface topographies at the start and end of fatigue loading cycles. In these images, dominant peaks are marked with solid boundary shapes and valleys are marked with dashed boundary shapes. Figure 7a, b exhibit the surface textures of FM-40-5 T at 0.5 and 30.5 loading cycles, respectively. These figures show that surface texture is perpendicular to the axial direction of the specimens. No clear features are apparent at 0.5 cycle while two dominant ridges and one pit are detected at 30.5 cycles. This deeper pit shows the formation of cracks nucleated from the valley of ridges. Figures 7c and d explicate the 3D surface textures of FM-40-5 T. At 0.5 loading cycle, comparatively smooth surface texture with minor undulations is detected than FM-40-5 T. Moreover, a uniform distribution of peaks and valleys is observed. At 30.5 cycles, two characteristics zones are spotted on the surface: one zone comprises clear ridges and the other zone consists of dales representing the formation of cracks. Surface topographic images for FB-49-5 T are shown in Figs. 7e and f. Blasted specimen represented irregular rough surface due to the wear and plastic deformation of the material. A number of significant pits and summits can also be seen without any periodical features, but no visible cracks are found on the topographic images of the blasted specimen due to its highest surface roughness. However, prominent cracks were physically detected by the naked eye on all the steel specimens at the end of fatigue loading cycles.

3.2.1 Calculation of 3D Surface Roughness Parameters

3D surface roughness parameters are effectively used for analyzing the characteristics of the processed surfaces [24]. The following seven roughness parameters are calculated here to describe the morphology of the steel surface at the start and end of fatigue loading cycles: S_a (arithmetic mean height of the surface), S_q (root mean square height of the surface), S_p (maximum height of peak), S_v (maximum depth of

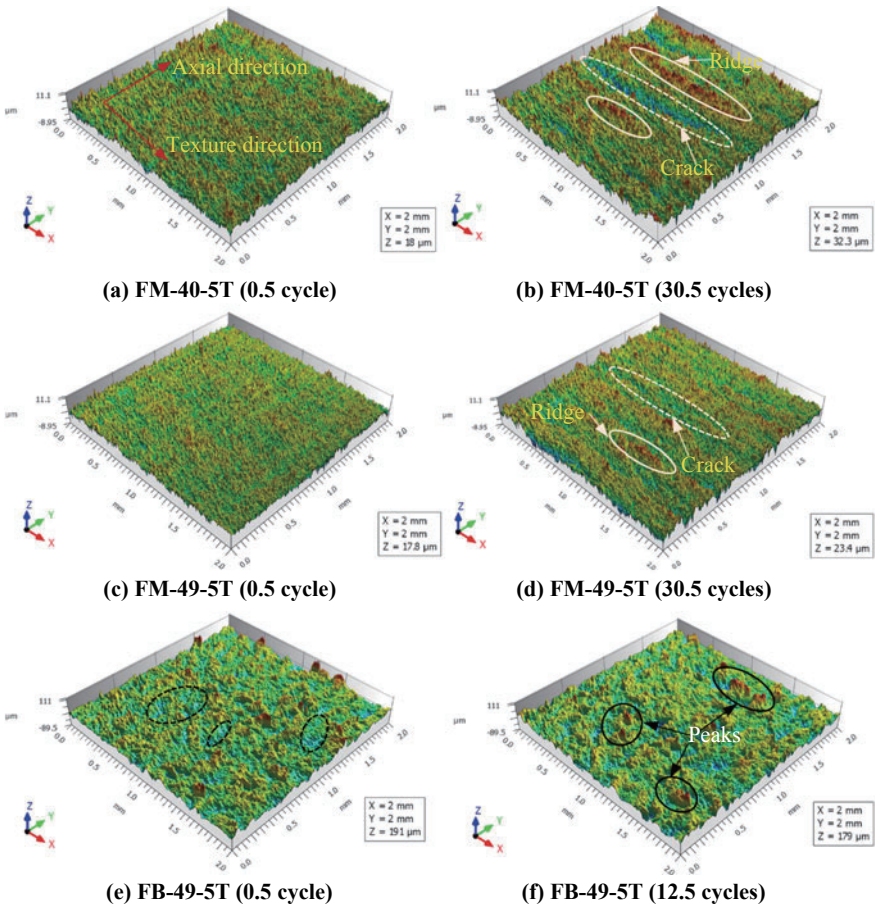

(a) FM-40-5T (0.5 cycle) **(b) FM-40-5T (30.5 cycles)**

(c) FM-49-5T (0.5 cycle) **(d) FM-49-5T (30.5 cycles)**

(e) FB-49-5T (0.5 cycle) **(f) FB-49-5T (12.5 cycles)**

Fig. 7 Surface topographic analyses at the start and end of loading cycles for all test specimens

valley), S_z (maximum surface profile height), S_{sk} (skewness), S_{ku} (kurtosis). For the evaluation of all the above parameters, an algorithm is developed by employing the programming language "MATLAB" [25] and the results are enlisted in Table 4.

The calculation results demonstrate that surface roughness increases with the increase in fatigue loading cycles. S_a value of FB-49-5 T is 6.38 and 7.51 times higher than FM-40-5 T and FM-49-5 T respectively. S_a, S_q, S_p, S_v and S_z parameters indicated an increase at the end of fatigue loading for mechanically polished specimens. But for the blasted specimen, S_p, S_v and S_z values showed a slight decrease at the end of fatigue loading due to the formation of micro pits as a result of the wear process.S_{sk} denotes the deviation of surface about the mean plane and this parameter is effectively used for describing the shape of surface height distribution [24]. S_{sk} values are positive for all the specimens representing the more height of ridges from the mean plane.S_{sk} represents the peakedness of surface height data and S_{ku} values

Table 4 3D surface roughness parameters at the start and end of fatigue loading cycles

Roughness parameters	FM-40-5 T		FM-49-5 T		FB-49-5 T	
	0.5 cycle	30.5 cycles	0.5 cycle	30.5 cycles	0.5 cycle	12.5 cycles
S_a (μm)	1.44	2.07	1.22	1.76	12.35	13.21
S_q (μm)	1.81	2.64	1.54	2.21	16.21	17.48
S_p (μm	10.20	17.84	10.18	10.95	102.93	93.61
S_v (μm)	7.80	14.44	7.60	12.47	87.75	85.31
S_z (μm)	17.99	32.28	17.77	23.42	190.68	178.92
S_{sk}	1.62	1.68	1.64	1.62	1.85	1.85
S_{ku}	3.13	3.44	3.21	3.16	4.46	4.33

for all the specimens are greater than 3 indicating the surface is distributed centrally with the occasional deep valleys or high peaks. With the comparison and use of the above calculated 3D surface roughness parameters, it is possible to differentiate the materials with variable surface treatments and the damage assessment can also be done considering the progressive change in surface roughness.

3.3 Finite Element Modeling of Notched Steel Specimens

In this study, the finite element (FE) software "Abaqus version 6.14" is employed to carry out the numerical simulation of notched steel specimens for the verification of the surface curvature method. Linear and nonlinear buckling analyses are performed by incorporating the material and geometric nonlinearities. The computation took hours on a 2.9 GHz PC. A schematic representation of the 3D finite element model of the notched specimen made by employing solid modeling technique is demonstrated in Fig. 8. Since the gripping region is around 40 mm, so for the simplification of the model, the remaining part is only used for conducting the analysis.

3.3.1 Material Properties

Numerical modeling is done on FM-40-5 T and FM-49-5 T specimens consisting of SM400A and SM490A steels. Since steel is a homogenous material, so the linear material properties are assigned to the model as elastic isotropic by defining the values of Poisson's ratio as 0.3, the density of 7850 kg/m^3 and young's modulus of 200 GPa. For defining the nonlinear behavior of the material, the rate-independent isotropic hardening plasticity model is adopted. The plastic data for both steel types are obtained from the tension test of coupon specimens.

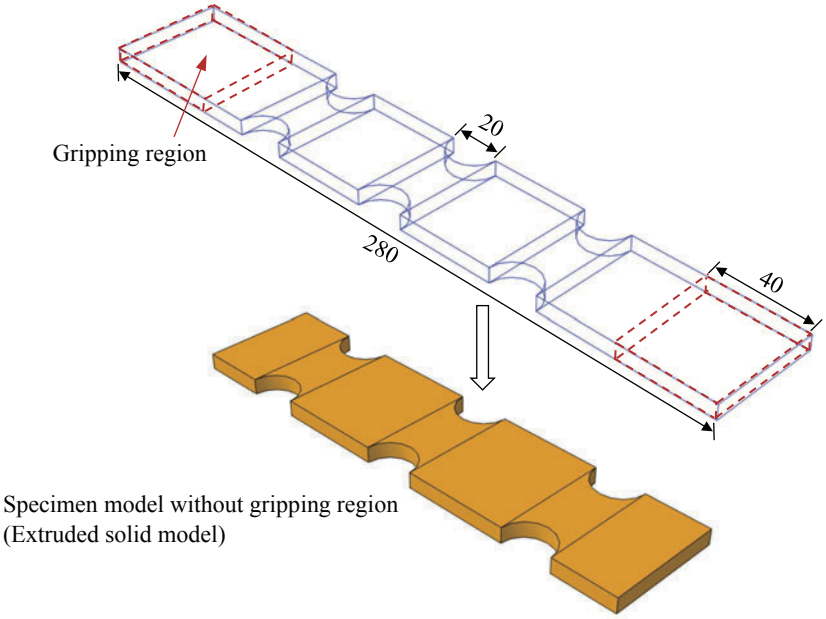

Fig. 8 FE model of notched steel specimen (all dimensions are in mm)

3.3.2 Loads and Boundary Conditions

To simulate the buckling phenomenon, displacement-controlled loading with an amplitude of 5 mm is applied at the top corner of the specimen and a tie constraint is provided for the load distribution from the corner to the whole top surface. Boundary conditions are applied to the specified regions of the model by restraining the movement in a particular degree of freedom. For the current study, it was difficult to correctly simulate the boundary conditions and the problem of instability can also arise in notched components. So, considering the expected buckling behavior, hinge supports are provided at the bottom by constraining the translational degrees of freedom (U_X, U_Y and U_Z) and the top part is free in the axial direction by the restraining U_Y and U_Z.

3.3.3 Meshing

For representing the steel section in the current analysis, solid elements are used for simulating the behavior of notched specimens under the application of axial load. The 3D solid model is discretized with a hexahedral mesh consisting of 8-node "C3D8R" elements with reduced integration to simulate the buckling behavior of global models. This element type is chosen because of its general usage in solving linear and nonlinear problems, and it also offers hourglass control. Based on the

results of convergence analysis, a mesh size of 1 mm is selected for the solid elements in order to achieve accuracy in simulation results.

3.3.4 Nonlinear Buckling Analysis

After defining the required parameters, FE models are developed, and nonlinear buckling analysis is done following two stages. In the first step, linear eigenvalue buckling analysis is performed to obtain the mode shapes and then the nodal coordinates for the desired mode shapes are written as an output for the next step. In the second step, nonlinear buckling analysis is executed by using the Static, General method by incorporating the material nonlinearity, and finally, the geometric imperfections are introduced corresponding to 1st eigenmode. Figure 9 depicts the flow chart containing the steps of conducting nonlinear buckling analysis.

The results of nonlinear buckling analysis after 0.5 loading cycle for "FM-40-5 T and FM-49-5 T" specimens are illustrated in Figs. 10 and 11. Figure 10 indicates that

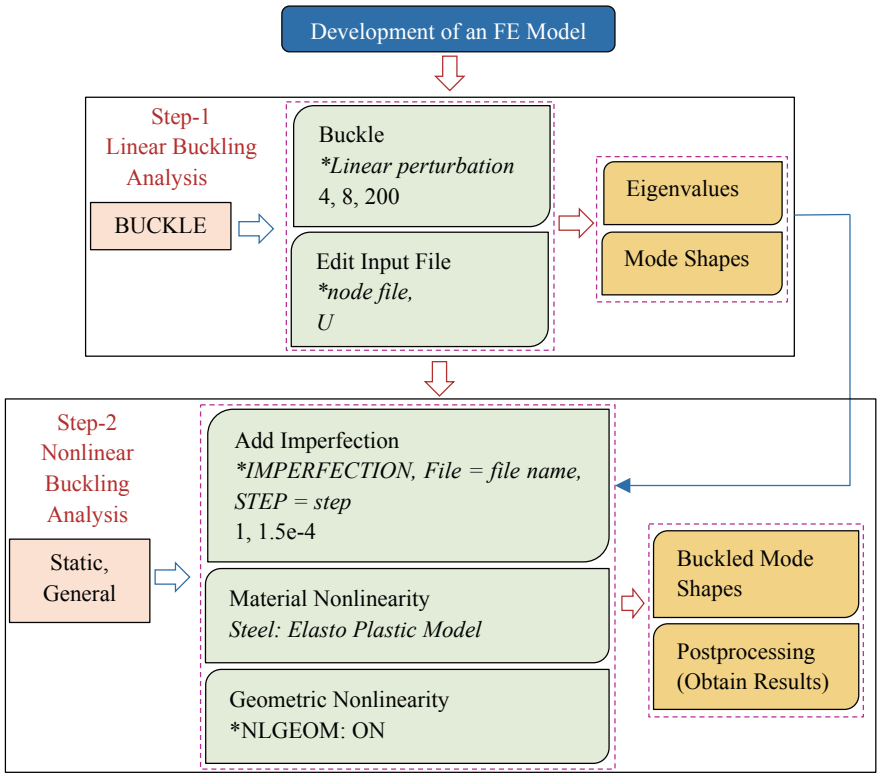

Fig. 9 Flow chart depicting the steps of conducting nonlinear buckling analysis in Abaqus

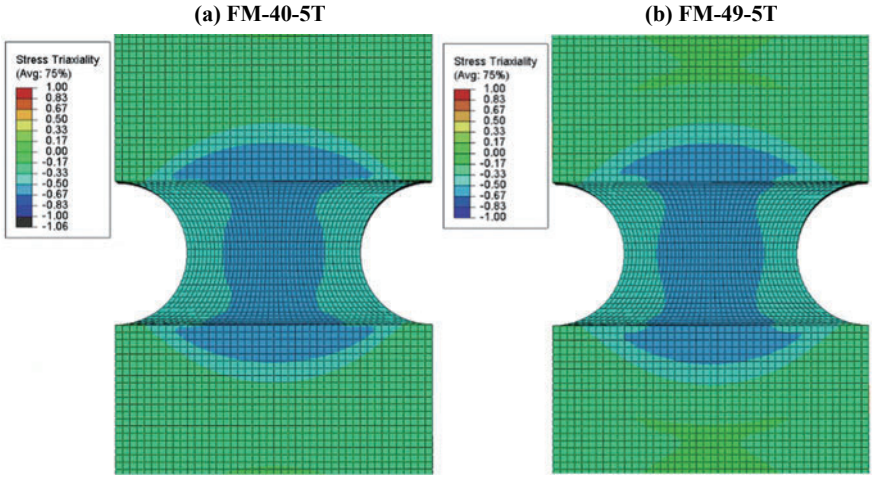

Fig. 10 Stress triaxiality at the center of **a** FM-40-5 T **b** FM-49-5 T specimens

there is a uniform distribution of stress triaxiality at the center of both the specimens on which the cracks are identified.

Figures 11a and b illustrate the equivalent plastic strain (PEEQ) distributions for "FM-40-5 T and FM-49-5 T" specimens, respectively along with the zoomed views of the central part of the specimens. Maximum plastic strain values of 16.06% and 15.85% are obtained at the central notches for FM-40-5 T and FM-49-5 T respectively. Since SM490A is high-strength steel, that is why the lesser strain is developed in FM-49-5 T. Also, there is a minor difference in plastic strain values for both the specimens concluding that the variable steel types have a minor influence on fatigue strength of steel than the effect of surface finish.

For the validation of the surface curvature method of strain evaluation, experimentally obtained strain values are compared with the numerical values. Strain values from the simulation are calculated on the compression side of the middle notch of the specimens (represented by cross sign in the above figures). The area in Fig. 11 with blue color is having PEEQ value equal to zero, indicating that the material is still having the elastic behavior. Table 5 highlights the comparison of numerical and experimental strain values calculated at the center of the middle notch after 0.5 loading cycle for FM-40-5 T and FM-49-5 T specimens. A difference in experimental and numerical strain values of about 6.30% and 11.0% is found for FM-40-5 T and FM-49-5 T, respectively. This might be due to ignoring the effects of axial strain and Poisson's ratio because the distance of the neutral axis from the surface keeps on changing due to the bending effect. Also, a minor difference in experimental and simulation results shows the validity of the proposed surface curvature method.

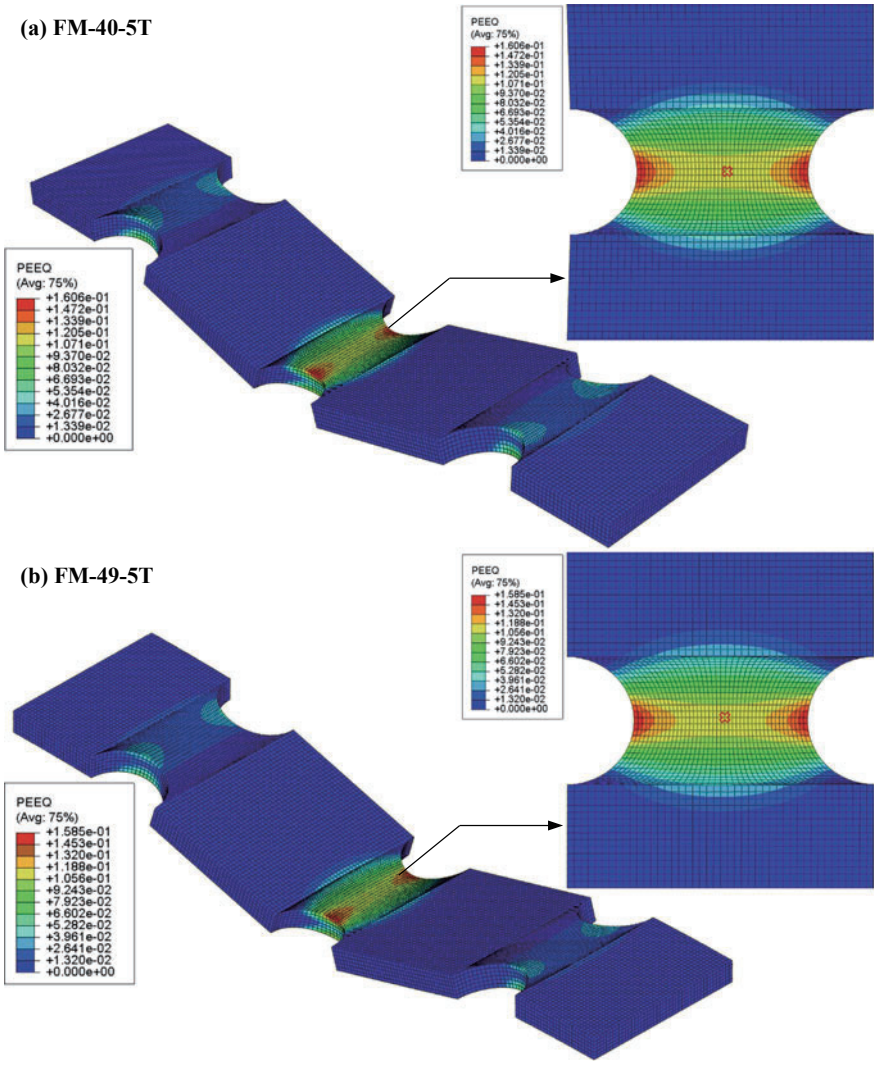

Fig. 11 Equivalent plastic strain distribution in **a** FM-40-5 T **b** FM-49-5 T specimens

Table 5 Comparison of numerical and experimental plastic strain values

Specimens	Strain from numerical analysis (%)	Strain from experimental data using surface curvature method (%)
FM-40-5 T	11.322	10.608
FM-49-5 T	11.237	10.000

4 Summary and Conclusions

This study deals with the topographic changes occurring on the steel surfaces undergoing cyclic plastic deformation. Three different types of specimens consisting of SM400A and SM490A steels with mechanically polished and blasted finishes are investigated. The topographic analysis is done for observing the variations in surface geometries at the start and end of fatigue loading cycles. The combined effects of surface finish and steel type on LCF life are also examined. Based on the experimental and simulation results, the following conclusions are drawn:

- From the experimentation, it is concluded that variable surface treatments significantly affect the process of crack initiation than the types of steel. In the case of the blasted specimen, cracks nucleated earlier at 12.5 cycles than the mechanically polished specimens on which cracks appeared at 30.5 cycles. Moreover, blasting treatment caused a reduction in fatigue strength, about 2.4 times that of mechanical polishing showing that the vulnerability of blasted surface to fatigue damage.
- The proposed surface curvature method is capable enough to evaluate the plastic strain from the surface height data. The validity of this method is verified by conducting numerical simulations on notched steel specimens.
- Strain histories depicted an increase in plastic strains with the progression in fatigue loading cycles due to the accumulation of residual plastic deformation. This increase can also be attributed to the increase in the number of microcracks formations and the growth of cracks.
- Evaluation of surface characterization parameters for all the three specimens depicted that the blasted specimen is having the highest value of average roughness. At the start of fatigue loading cycles, surface textures represented very minor undulations, while at the end of loading cycles, all the specimens showed a significant variation in surface topographies.
- The results of nonlinear finite element analysis are in good agreement with the experimental results indicating that numerical simulation is efficient enough to produce the same buckling behavior as detected in the experiment. Also, a slight difference in numerically and experimentally obtained plastic strain values confirms the validity of the proposed surface curvature method.

References

1. Cui W (2002) A state-of-the-art review on fatigue life prediction methods for metal structures. J Mar Sci Technol 7:43–56. https://doi.org/10.1007/s007730200012
2. Xue L (2008) A unified expression for low cycle fatigue and extremely low cycle fatigue and its implication for monotonic loading. Int J Fatigue 30:1691–1698. https://doi.org/10.1016/j.ijfatigue.2008.03.004

3. AM Kanvinde GG Deierlein 2005 Continuum based micro-models for ultra low cycle fatigue crack initiation in steel structures Struct Congr 1–11https://doi.org/10.1061/40753(171)192
4. Miki C, Aizawa T, Anami K (1998) Brittle fracture at beam-to-column connection during earthquake. J JSCE 591 (I–43):273–281. https://doi.org/10.2208/jscej.1998.591_273
5. Wei W, Han L, Wang H et al (2017) Low-Cycle fatigue behavior and fracture mechanism of HS80H steel at different strain amplitudes and mean strains. J Mater Eng Perform 26:1717–1725. https://doi.org/10.1007/s11665-017-2575-0
6. Tamura H, Sasaki E, Hitoshi Y, Katsuchi H (2012) Study on the casue of brittle fracture during earthquakes in steel bridge bents focusing on dynamic load effect. J JSCE 68:226–241. https://doi.org/10.2208/jscejseee.68.226
7. H Tamura E Sasaki S Tominaga 2018 Modified-Weibull-stress-based evaluation of brittle fracture occurrence during earthquakes in steel members Eng Fract Mech 202 375 393https://doi.org/10.1016/j.engfracmech.2018.08.005
8. Nakashima M, Inoue K, Tada M (1998) Classification of damage to steel buildings observed in the 1995 Hyogoken-Nanbu earthquake. Eng Struct 20:271–281. https://doi.org/10.1016/S0141-0296(97)00019-9
9. Miller DK (1998) Lessons learned from the Northridge earthquake. Eng Struct 20:249–260. https://doi.org/10.1016/S0141-0296(97)00031-X
10. Miner MA (1945) Cummulative damage in fatigue. J Appl Mech 12:A159–A164. https://doi.org/10.1115/1.4009458
11. Tateishi K, Hanji T, Minami K (2007) A prediction model for extremely low cycle fatigue strength of structural steel. Int J Fatigue 29:887–896. https://doi.org/10.1016/j.ijfatigue.2006.08.001
12. Sinsamutpadung N, Sasaki E, Tamura H (2016) Effects of high strain rate on low-cycle fatigue behavior of structural steel in large plastic strain region. J JSCE 4:118–133. https://doi.org/10.2208/journalofjsce.4.1_118
13. Bayoumi MR, Abdellatif AK (1995) Effect of surface finish on fatigue strength. Eng Frcature Mech 51:861–870. https://doi.org/10.1016/0013-7944(94)00297-U
14. Al-Shahrani S, Marrow TJ (2009) Effect of surface finish on fatigue of stainless steels. In: 12th International Conference on Fracture 2009, ICF-12. pp 861–870
15. Maiya PS, Busch DE (1975) Effect of surface roughness on low-cycle fatigue behavior of type 304 stainless steel. Metall Trans A 6:1761–1766. https://doi.org/10.1007/BF02642305
16. Xiao WL, Chen HB, Yin Y (2012) Effects of surface roughness on the fatigue life of alloy steel. Key Eng Mater 525–526:417–420. https://doi.org/10.4028/www.scientific.net/KEM.525-526.417
17. Y Gao W Yang Z Huang Z Lu 2021 Effects of residual stress and surface roughness on the fatigue life of nickel aluminium bronze alloy under laser shock peening Eng Fract Mech 244https://doi.org/10.1016/j.engfracmech.2021.107524
18. Leidermark D, Moverare J, Simonsson K et al (2010) Fatigue crack initiation in a notched single-crystal superalloy component. Procedia Eng 2:1067–1075. https://doi.org/10.1016/j.proeng.2010.03.115
19. Hsu TY, Wang Z (2010) Fatigue crack initiation at notch root under compressive cyclic loading. Procedia Eng 2:91–100. https://doi.org/10.1016/j.proeng.2010.03.010
20. JIS G 3106 (2004) Rolled steels for welded structure. Japanese Standards Association
21. Zhao B, Liu T, Chen J et al (2019) A new Bernoulli-Euler beam model based on modified gradient elasticity. Arch Appl Mech 89:277–289. https://doi.org/10.1007/s00419-018-1464-9
22. Jouini N, Gautier A, Revel P et al (2009) Multi-scale analysis of high precision surfaces by Stylus Profiler, Scanning White-Light Interferometry and Atomic Force Microscopy. Int J Surf Sci Eng 3:310. https://doi.org/10.1504/IJSURFSE.2009.027418
23. Le Roux S, Deschaux-Beaume F, Cutard T, Lours P (2015) Quantitative assessment of the interfacial roughness in multi-layered materials using image analysis: Application to oxidation in ceramic-based materials. J Eur Ceram Soc 35:1063–1079. https://doi.org/10.1016/j.jeurceramsoc.2014.09.027

24. Zeng Q, Qin Y, Chang W, Luo X (2018) Correlating and evaluating the functionality-related properties with surface texture parameters and specific characteristics of machined components. Int J Mech Sci 149:62–72. https://doi.org/10.1016/j.ijmecsci.2018.09.044
25. MATLAB. Version 9.3.0.713579 (R2017) Natick: The MathWorks Inc. 2017